Improved Detection of Hepatic Metastases with Contrast-enhanced Low Mechanical-index Pulse Inversion Ultrasonography During the Liver-specific Phase of Sonazoid:

Observer Performance Study with JAFROC Analysis[1]

Katsutoshi Sugimoto, MD, Junji Shiraishi, PhD, Fuminori Moriyasu, MD, Kazuhiro Saito, MD, Kunio Doi, PhD

Rationale and Objectives. To compare B-mode ultrasonography (US) alone with the combination of B-mode and contrast-enhanced (Sonazoid) late-phase pulse-inversion US for the detection of hepatic metastases by use of jackknife free-response receiver-operating characteristic (JAFROC) analysis.

Materials and Methods. Twenty-seven patients with 57 hepatic metastases and 6 patients without hepatic metastases underwent B-mode and contrast-enhanced US. We used the diagnoses established by contrast-enhanced computed tomography and contrast-enhanced US as the standard of reference. All ultrasonographic scanning was performed by an experienced radiologist with a routine clinical procedure. All scanning data were archived with digital cine clips. A review system, which can display pairs of cine clips for B-mode and contrast-enhanced US side by side, was developed for off-site observer study. Seven radiologists interpreted each case individually first by B-mode US only, and then by the combination with contrast-enhanced US by identifying locations of possible candidates for hepatic metastasis with their confidence ratings. The figure-of-merit (FOM) values, sensitivity, and false-positives per case were estimated for B-mode US alone, and for the combination of B-mode and contrast-enhanced US.

Results. The sensitivities of the combined ultrasonographic imaging (mean, 72.2%) were clearly improved from that of B-mode US alone (mean, 41.6%) while reducing the average number of false positives from 1.1 to 0.5 per case. In the jackknife analysis, there was a statistically significant difference between mean FOM values for the combined imaging (0.76) and for B-mode US alone (0.44, $P < .00001$).

Conclusion. Evaluating cine clips of contrast-enhanced liver US together with B-mode US could improve physicians' accuracy for detection of hepatic metastases.

Key Words. Ultrasonography; contrast media; sonazoid; detection; liver metastasis; free-response receiver-operating characteristic; observer performance study.

Acad Radiol 2009; 16:798–809

[1] From the Kurt Rossmann Laboratories for Radiologic Imaging Research, Department of Radiology, The University of Chicago, 5841 S. Maryland Ave., MC 2026, Chicago, IL 60637 (K. Sugimoto, J.S., K.D.); Department of Gastroenterology and Hepatology, (K. Sugimoto, F.M.), and Department of Radiology (K. Saito), Tokyo Medical University, Tokyo, Japan. Received November 18, 2008; accepted December 24, 2008. **Address correspondence to:** K. Sugimoto. e-mail: sugimoto@comcast.net

doi:10.1016/j.acra.2008.12.025

The liver is one of the most common sites for metastases, and the detection of metastases is crucially important because of therapeutic and prognostic implications. Accurate staging is a prerequisite for successful surgery and for monitoring of chemotherapy. Because the sensitivity of conventional ultrasonography (US) for hepatic metastases was relatively poor (53%–77%) (1–3), contrast material-enhanced computed tomography (CT) and magnetic resonance (MR) imaging have been recommended for the detection of liver metastases.

It has been reported that the advent of the microbubble contrast agent SHU 508A (Levovist; Schering, Berlin, Germany) and the development of a gray-scale microbubble-specific ultrasonographic technique, which was called pulse- or phase-inversion harmonic contrast enhanced US, has remarkably improved the detection of liver metastases by use of US (4–7). However, contrast-enhanced US with SHU 508A is limited because prolonged evaluation of liver contrast enhancement cannot be performed due to a technical factor (8).

A second-generation ultrasonographic contrast agent NC100100 (Sonazoid; GE Healthcare, Oslo, Norway) became clinically available in January 2007 in Japan ahead of other countries. Advances in contrast-enhanced US by use of a low mechanical index and the new contrast agent have enabled real-time assessment of contrast enhancement with minimal microbubble destruction. The agent, especially, is known to have hepatic parenchyma-specific contrast during the delayed phase, in which malignant tumors appear as clear signal voids without enhancement; thus, the detection of lesions has been improved. In addition, signal enhancement in the parenchyma commonly lasted for 120 minutes compared to rapid decay (5–10 minutes) in vessels (9–11). Contrast-enhanced (NC100100) late-phase pulse-inversion US, therefore, is expected to improve the detection of hepatic metastases in clinical practice.

The problem encountered with every ultrasonographic examination, however, is its operator-dependent nature, compared to CT and MR imaging. Therefore, for further prevailing US examinations, it is necessary to reduce the operator-dependent limitations of US. To this end, as in CT and MR imaging, we believe that it is necessary to transmit US image data to another room for diagnosis, and a dedicated diagnostic workstation should be developed for radiologists' image interpretation. For example, real-time three-dimensional (3D) US (12) has been applied to clinical practice, and it has become easy to obtain volume data, which has been common in CT and MR imaging, and thus reproducible and consistent ultrasonographic images for diagnosis can be realized with less dependence on the operator. To demonstrate the diagnostic capability of ultrasonographic images in off-site reading, it would be useful to investigate whether physicians can detect liver metastases visualized by use of a workstation, as a part of our observer performance study.

Although the detection of liver metastases by US has been examined to date, subjective diagnosis by the sonologist in charge of the ultrasonographic examination has been commonly used in all previous reports (4–7,13). In the present study, ultrasonographic digital cine clips taken by one radiologist were examined by seven observers in an observer performance study. To our knowledge, this is the first report of an observer performance study on the detection of hepatic metastases based on off-site reading of ultrasonographic digital cine clips.

Our purpose in this study was to compare the accuracy of conventional B-mode US with that of the combination of conventional B-mode US and contrast-enhanced (NC100100) late-phase pulse-inversion US in the detection of hepatic metastases by using jackknife free-response receiver-operating characteristic (JAFROC) analysis with seven observers.

MATERIALS AND METHODS

This prospective study was approved by the research ethics board of our institution; informed consent was obtained from each patient for the use of ultrasonographic data for research purposes, and from each observer for participating in the observer performance study.

Patients and Reference Standards

Sixty-seven patients underwent contrast-enhanced US for evaluation of liver metastases at our department between January 2007 and October 2007. For 56 of these patients, contrast-enhanced CT with a multidetector row scanner, B-mode US, contrast-enhanced US, and superparamagnetic iron oxide (SPIO)-enhanced MR imaging were performed within 30 days. Nineteen of the 56 patients were excluded from our study because five patients were undergoing chemotherapy during this period, and because 14 patients had too many nodules (i.e., more than 10 in one patient) to be analyzed. Patients were recruited prior to undergoing baseline US, and, once recruited, a patient could not be excluded on the basis of poor technical quality of the ultrasonographic examination. This was done to avoid selection bias in favor of patients who may provide good-quality ultrasonographic images. The remaining 37 patients (21 men and 16 women) were included in this study. The mean age was 69.5 years (range, 44–89 years).

Eight of the 37 patients had no hepatic metastases, as confirmed with follow-up imaging studies performed over the course of at least 6 months (range, 6–17 months). The remaining 29 patients had hepatic metastases. The primary cancer sites in each patient were as follows: 16 colorectal cancers, five gastric cancers, three ovary cancers, one bladder cancer, one lung cancer, one uterine cancer, one carcinoid of the duodenum, and one bile duct cancer.

The presence or absence of hepatic metastases was decided in consensus by two radiologists with 18 and 9 years of experience, respectively, in hepatobiliary imaging who were not included among the seven blinded readers for the observer study. The consensus was made based on the findings obtained with contrast-enhanced CT, B-mode US, contrast-enhanced US, and SPIO-enhanced MR imaging; findings obtained at follow-up US, CT, and MR imaging; and findings obtained at surgery and percutaneous biopsy.

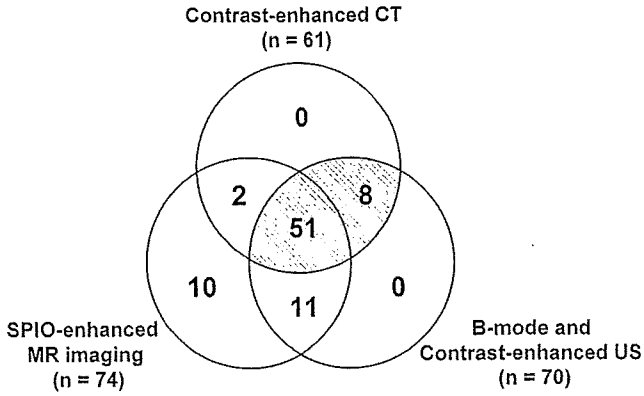

Figure 1. Confirmation of 82 hepatic metastases and "gold standard" used in this study. CT, computed tomography; MR, magnetic resonance; US, ultrasonography.

Three of the 29 patients underwent surgery and five patients had percutaneous biopsy within 30 days after CT, SPIO MR imaging, and US. Seventeen metastases were confirmed histologically in these eight patients. The 65 visible hepatic tumors in the remaining 21 patients for whom histopathologic confirmation of disease was not available were considered as having hepatic metastases on the basis of tumor growth observed at follow-up examination (performed 2–17 months after US, CT, or MR imaging). The follow-up examinations revealed no other liver metastases in these patients. There were no patients with hepatic cirrhosis in this study. Hepatic cirrhosis was diagnosed with liver function tests or morphologic findings on US, CT, or MR imaging.

As a result, 82 hepatic metastases (mean diameter, 13.5 mm; range, 2.0–77.2 mm) were confirmed for 29 of the 37 patients. The number, size, and location of the metastases were documented on a segmental basis (Couinaud's (14) and Bismuth's (15) classification) on schematic liver charts for each imaging modality. Of the 82 hepatic metastases, 74 were identified by SPIO-enhanced MR imaging, 61 by contrast-enhanced CT, and 70 by B-mode and contrast-enhanced US. These results are illustrated in Figure 1. Note that these results were not obtained based on blinded observer studies; therefore, relative advantages of the modalities could not be discussed based on the number of identified liver metastases in Figure 1.

Regarding benign lesions, 25 of the 37 patients had 68 cysts; the number of cysts was documented. In this study, only one patient had more than 20 cysts, and a numeric value of 21 was used for analysis. Five of the 37 patients had seven liver hemangiomas, and six patients had 10 focal fatty sparings and focal fatty changes. In patients with cancer who were treated with chemotherapy, the liver is often heterogeneous, and suspicious findings are usually detected on B-mode US. In this study, we diagnosed these lesions as fibrosis or sequelae (13). Eight of the 37 patients had 30 such lesions.

The diagnosis of cysts was determined by means of typical findings at US, heavily T2-weighted MR imaging, contrast-enhanced CT, and also based on no change in lesion size for 6 months or more (16,17). The diagnosis of hemangioma was determined by means of typical findings at US, typical enhancement at dynamic contrast-enhanced CT, and no change in lesion size for 6 months or more (18,19). The diagnosis of focal fatty change and focal fatty sparing was determined by means of typical findings at US, MR imaging with opposed-phase gradient-echo sequence, the fat-saturation technique, and no change in lesion size for 6 months or more (20–21). The diagnosis of fibrosis or sequelae was determined by means of US, and by no change in lesion size for 6 months or more.

Table 1
Sizes of 57 Hepatic Metastases

Diameter (mm)	No. of Lesions
Less than or equal to 5	10 (17.5 %)
6–10	18 (31.6 %)
11–20	16 (28.1 %)
Greater than or equal to 21	13 (22.8 %)

For training observers to become familiar with the procedure and the interface of the observer study, two cases with two nodules were selected based on the criteria, namely, the cases were not too easy and not too difficult for diagnosis, and the combination of one "easy" case and another "difficult" case. In addition, we excluded two normal cases that looked obviously normal.

Consequently, the remaining 33 patients (27 patients with metastasis and six normal cases) were included in this study; we finally selected 57 hepatic metastases (mean diameter, 16.2 mm; range, 2.5–77.2 mm), which were identified by both contrast-enhanced CT and contrast-enhanced US as the gold standard. The distribution of the size and the number of lesions is shown in Table 1. Regarding other benign lesions, 22 of the 33 patients had 64 cysts, five had seven liver hemangiomas, six had 10 focal fatty sparings and focal fatty changes, and eight had 30 fibroses or sequelae.

Ultrasonographic Examination Technique

Both pre- and postcontrast US were performed by a radiologist, who has seven years of experience in microbubble contrast material-enhanced US of the liver. The radiologist was aware of the patients' clinical histories, and was blinded to the all other imaging findings. All scanning was performed using a SSA-790A (Aplio XG; Toshiba Medical Systems Corp., Otawara, Japan) with a 3.75-MHz convex transducer (PVT-375BT). The imaging mode was wideband harmonic imaging (commercially called Pulse subtraction) with transmission and reception frequencies of 3.75 and 7.5 MHz, respectively.

Initially, patients underwent thorough first conventional baseline US in fundamental B-mode with a routine clinical

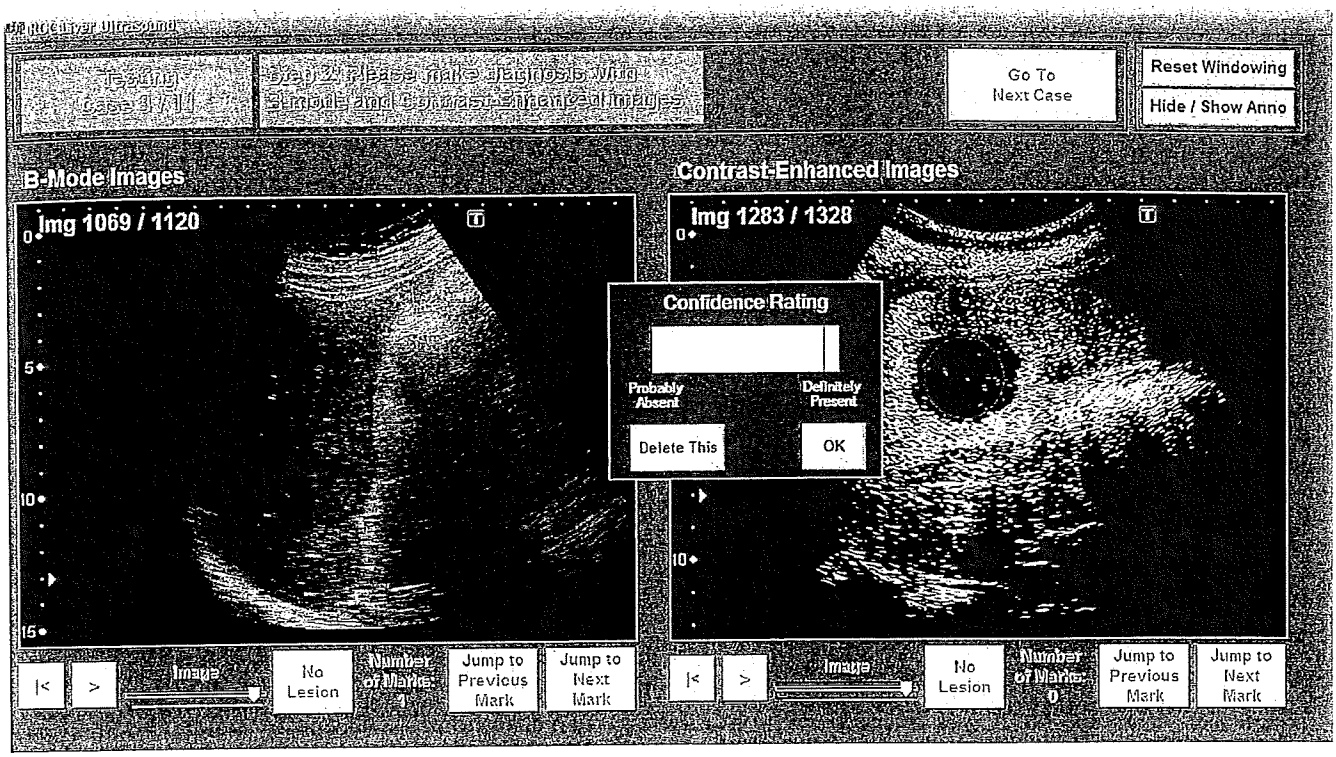

Figure 2. Overview of the observer study interface.

procedure and individually optimized scanner settings. A bolus of 0.5 mL of NC100100 was then injected by hand via a 22-gauge intravenous cannula at a rate of approximately 1 mL/s, followed by a 10-mL normal saline flush. No additional NC100100 bolus injections were given. The contrast agent consisted of perflubutane microbubbles surrounded by phospholipids. The average diameter of the microbubbles is 2 to 3 μm. Contrast-enhanced scanning was started 10 minutes after injection by use of pulse-inversion harmonic US with a low mechanical index (MI) (<0.3), which preserves the microbubbles and then allows real-time exploration of the liver. Contrast-enhanced scanning was conducted with a routine clinical procedure and individually optimized scanner settings. All scanning data were archived with digital cine clips for offline observer study. The cine clips were audio video interleave (AVI) format, each of which had 20 seconds. We have used from 24 to 30 AVI files per patient in this study, which included both B-mode and contrast-enhanced images.

For images to be used in the observer study, the radiologist removed unnecessary images from the collected ultrasonographic images in which the liver was not scanned and those likely to cause a bias for the observers in which suspected lesions were scanned repeatedly or with magnification.

Other Examination Techniques

Reference imaging examinations were performed within 30 days (mean, 10 days) of the day of ultrasonographic examinations. These reference examinations were contrast-enhanced multi-detector row CT (n = 33) and SPIO-enhanced MR imaging (n = 33). CT and MR imaging were performed as part of the clinical workup of the patients—in several cases outside our institution (CT [n = 4], MR imaging [n = 3])—and not for the purpose of this study. The imaging protocols

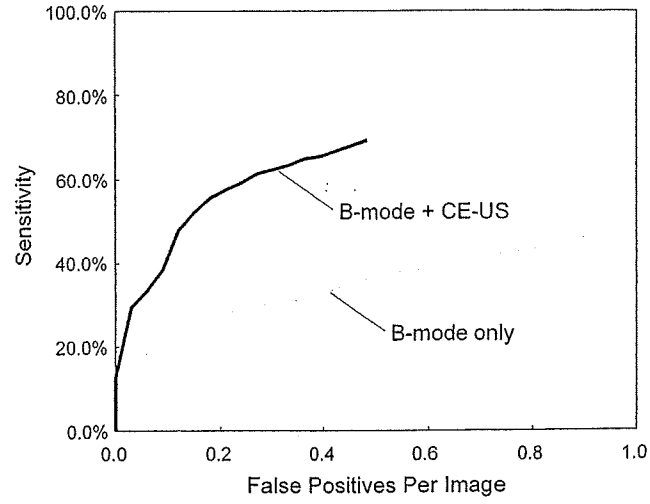

Figure 3. The average free-response receiver-operating characterstic curves show the increase in diagnostic performance after review of contrast-enhanced (CE)-ultrasonographic (US) images (*black line*).

Table 2
Sensitivity, FPs/case, and FOM Values in Detection of Hepatic Metastases

Reader	B-mode US Alone			Combined US Imaging		
	Sensitivity	FP / Case	FOM	Sensitivity	FP / Case	FOM
A	31.6 % (18/57)	0.24 (8/33)	0.33	57.9 % (33/57)	0.21 (7/33)	0.66
B	56.1 % (32/57)	1.97 (65/33)	0.55	79.0% (45/57)	0.45 (15/33)	0.82
C	38.6 % (22/57)	1.30 (43/33)	0.39	64.9 % (37/57)	0.64 (21/33)	0.66
D	36.8 % (21/57)	0.85 (28/33)	0.39	71.9 % (41/57)	0.52 (17/33)	0.78
E	50.9 % (29/57)	1.15 (38/33)	0.51	91.2 % (52/57)	0.55 (18/33)	0.93
F	38.6 % (22/57)	0.94 (31/33)	0.46	64.9 % (37/57)	0.33 (11/33)	0.74
G	38.6 % (22/57)	0.97 (32/33)	0.44	75.4 % (43/57)	0.52 (17/33)	0.76
Average	41.6 % (166/399)	1.06 (245/231)	0.44	72.2 % (288/399)*	0.46 (106/231)†	0.76‡

Combined US imaging, combination of B-mode and contrast-enhanced US; FOM, figure of merit; FP, false-positive; US, ultrasonography.
* The difference in mean sensitivity between B-mode US alone and the combination of B-mode US and contrast-enhanced US for all lesions was significant ($P < .00001$).
† The difference in mean FP/case between B-mode US alone and the combination of B-mode US and contrast-enhanced US for all lesions was significant ($P = .0132$).
‡ The difference in mean FOM value between B-mode US alone and the combination of B-mode US and contrast-enhanced US for all lesions was significant ($P < .00001$).

were therefore not standardized. Minimum requirements for CT were the use of a multidetector row computed tomographic scanner, and portal-venous phase images at 5-mm slice thickness with sufficient contrast enhancement as judged by the radiologist. SPIO-enhanced MR imaging consisted of diffusion-weighted (DW) sensitivity encoding (SENSE) imaging, T2-weighted fast spin-echo (SE) MR imaging, dual-echo, T1-weighted fast field-echo (FFE) MR imaging, and contrast-enhanced T2*-weighted imaging (6-mm slice thickness).

Observer Performance Study

We used a sequential test method (22) for reading first on B-mode ultrasonographic images without and then with contrast-enhanced ultrasonographic images by each physician. In the sequential test method, B-mode ultrasonographic images alone were shown first on the left monitor. Physicians were asked to indicate the presence and location of liver metastases, and then to mark their confidence level regarding the likelihood of liver metastases using a continuous rating scale displayed on the monitor (23). After the physician indicated all liver metastases and marked the initial level of confidence, the contrast-enhanced ultrasonographic images were shown on the right whereas B-mode ultrasonographic images were kept on the left. The physician was asked again to indicate liver metastases, and to mark the confidence level in the same way. An overview of the interface is shown in Figure 2.

The B-mode images and the combination of B-mode and contrast-enhanced US were interpreted independently by seven readers with 15, 20, 9, 8, 7, 9, and 15 years of experience, respectively, in liver ultrasonographic imaging. Each physician had at least 5 years of experience in microbubble contrast-enhanced US of the liver. Two radiologists who had determined the presence or absence of tumors on the basis of radiologic and pathologic findings were not included among the seven readers. All images were interpreted on a color LCD monitor (Flex Scan S1961-S; EIZO, Ishikawa, Japan).

Table 3
Averaged Number of False-positive Lesions by Seven Readers

Lesions	False-positive	
	B-mode No.	Combined US Imaging No.
Fibrosis or sequelae	23.9 (167/7)	5.0 (35/7)
Focal fatty sparing and focal fatty change	2.4 (17/7)	0 (0/7)
Cyst	5.9 (41/7)	9.9 (69/7)
Hemangioma	2.9 (20/7)	0.3 (2/7)
Total	35.0 (245/7)	15.1 (106/7)

Data in parentheses are the numbers used for calculating the averaged number of false-positive lesions per reader.

To hold observers' attention and avoid fatigue during the reading session, we divided the 33 cases into three sets (11 cases × 3 sets) so that one session would not take longer than 60 minutes. The distribution of cases with malignancy and normal cases for each set was the same: each set (11 cases) consisted of nine cases with liver metastases and two normal cases. Cases in each of the three sets were balanced comparable by the radiologist in the difficulty in the detection of liver metastases.

Written instructions were given to each physician for the observer study 1) The aim of this observer performance study is to investigate the utility of contrast-enhanced US in the

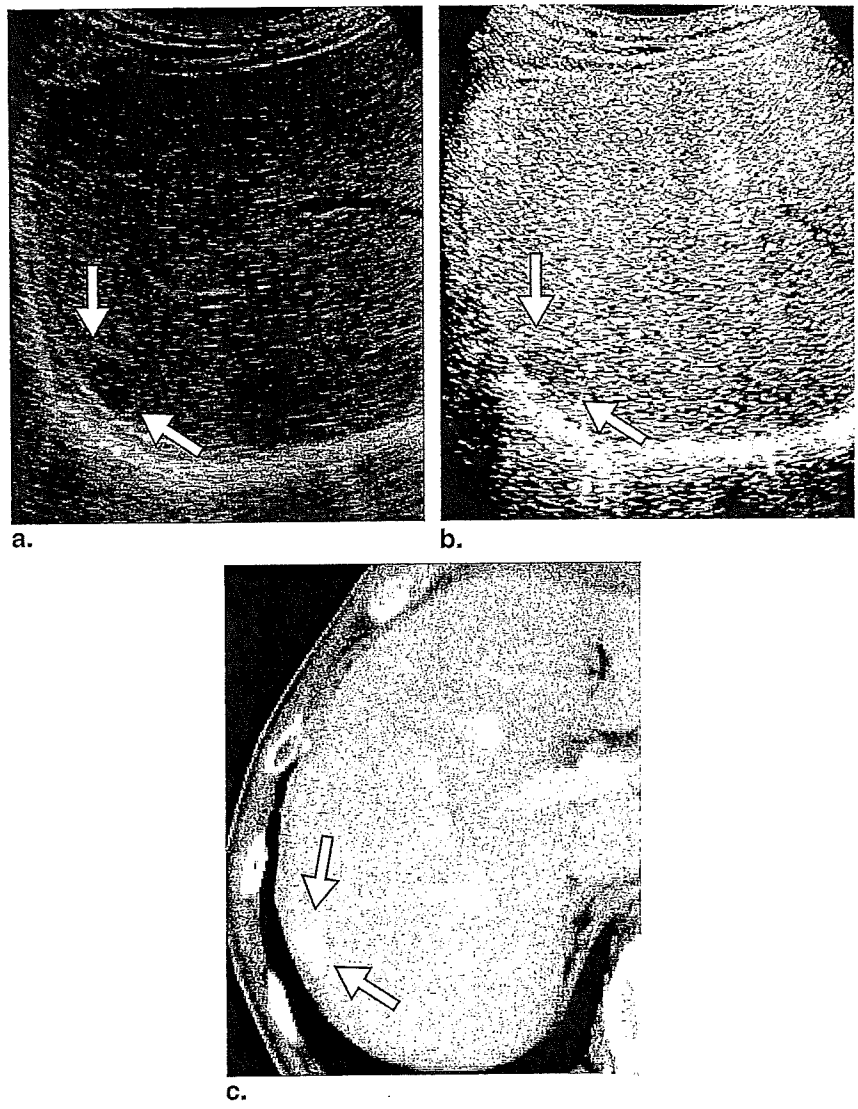

Figure 4. Liver hemangioma in a 65-year-old man. At follow-up computed tomography (CT) 6 months later, the lesion showed no change in size and typical enhancement on dynamic contrast-enhanced CT. Hence, the lesion was considered to be a liver hemangioma. **(a)** B-mode ultrasonographic (US) image obtained in the right lobe of the liver shows a hypoechoic lesion with marginal hyperechoic area. **(b)** Contrast-enhanced US image in the same region shows a slightly hypoechoic lesion compared to surrounding liver parenchyma, but shows late-phase uptake of contrast agent. **(c)** Transverse contrast-enhanced computed tomographic scan shows a hyperattenuating lesion. With B-mode US images alone, four readers detected the lesion as liver metastasis with high confidence level. With the combination of B-mode ultrasonography and contrast-enhanced US images, only one reader detected the lesion as liver metastasis with low confidence level.

detection of liver metastases and compare it to that of B-mode US alone. 2) The observer study consists of three sets. Each set is composed of 11 cases and two training cases, which are used for learning how to operate the interface. 3) Identify the location of all suspicious lesions by clicking a mouse, and then determine the confidence level for the presence of liver metastases on the bar in the window. The left and right ends of the bar correspond to the confidence level of "definitely absent" and "definitely present," respectively. 4) After all interpretations on B-mode images, display contrast-enhanced ultrasonographic cine clips on the right. 5) By using contrast-enhanced ultrasonographic images, repeat the same procedure (3). 6) There is no time limit in reading images. 7) Try to use the rating scale consistently and uniformly throughout all cases. 8) All displayed cine clips are edited to display only cine clips recorded according to the routine protocol for the

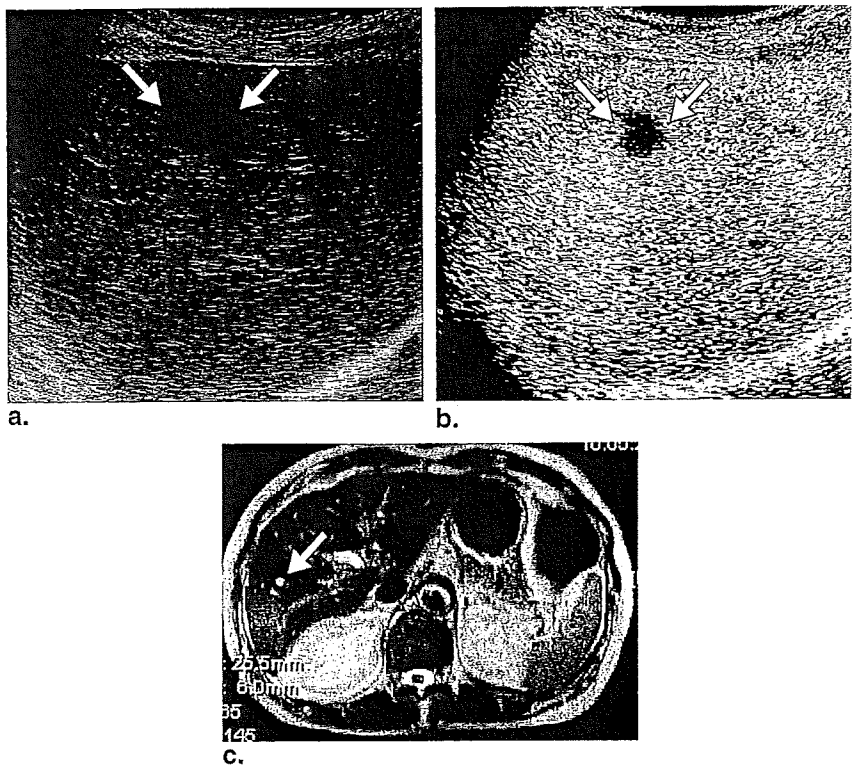

Figure 5. Liver cyst in a 73-year-old woman. At follow-up magnetic resonance (MR) imaging 6 months later, the lesion showed no change in size and typical findings on contrast-enhanced computed tomography. Hence, the lesion was considered to be a liver cyst. **(a)** B-mode ultrasonographic (US) image obtained in the right lobe of the liver shows a typical hepatic cyst with sharp margins and increased transmission through the lesion. **(b)** Contrast-enhanced US image in the same region shows subtle endocystic enhancing septa and slightly hyperechoic content. **(c)** Transverse precontrast heavy T2-weighted fast spin echo MR image shows the cyst as a very bright lesion. With B-mode US images alone, no reader detected the lesion as liver metastasis. Conversely, with the combination of B-mode US and contrast-enhanced US images, five readers detected the lesion as liver metastasis with high confidence level.

observer study. 9) The primary sites for the liver metastases include gastric, colorectal, uterine, lung, and urinary bladder cancers. 10) The presence or absence of all liver metastases should be confirmed by CT or MR imaging.

Statistical Analysis

We employed JAFROC analysis (24) to evaluate physicians' performance in the detection of hepatic metastases in B-mode ultrasonographic images without and with contrast-enhanced ultrasonographic images. The JAFROC analysis has been proposed for estimating a statistically significant difference in the detection of lesions with location. The JAFROC analysis is based on a free-response receiver-operating characteristic (FROC) paradigm and accounts for reader variation (25). Conventional receiver-operating characteristic (ROC) analysis is limited for this kind of application because each case receives only one response, although there are many possible hepatic metastases on each of the images; moreover, the information on the location of each of the hepatic metastases and the physicians' marks cannot be taken into account in the evaluation (26), whereas FROC analysis allows one to evaluate physicians' performance in diagnosing medical images by using multiple responses, each with information on the confidence level and location (24). For FOM value (27), the sensitivity, the number of false-positives per case, and the statistical significance of any difference between B-mode US alone and the combination of B-mode US and contrast-enhanced US were assessed by use of the Jackknife method (28). A P value $< .05$ was considered to indicate a statistically significant difference.

RESULTS

JAFROC Analysis

The physicians' performance in the detection of hepatic metastases in B-mode US without and with contrast-enhanced US is illustrated by the average FROC curves in

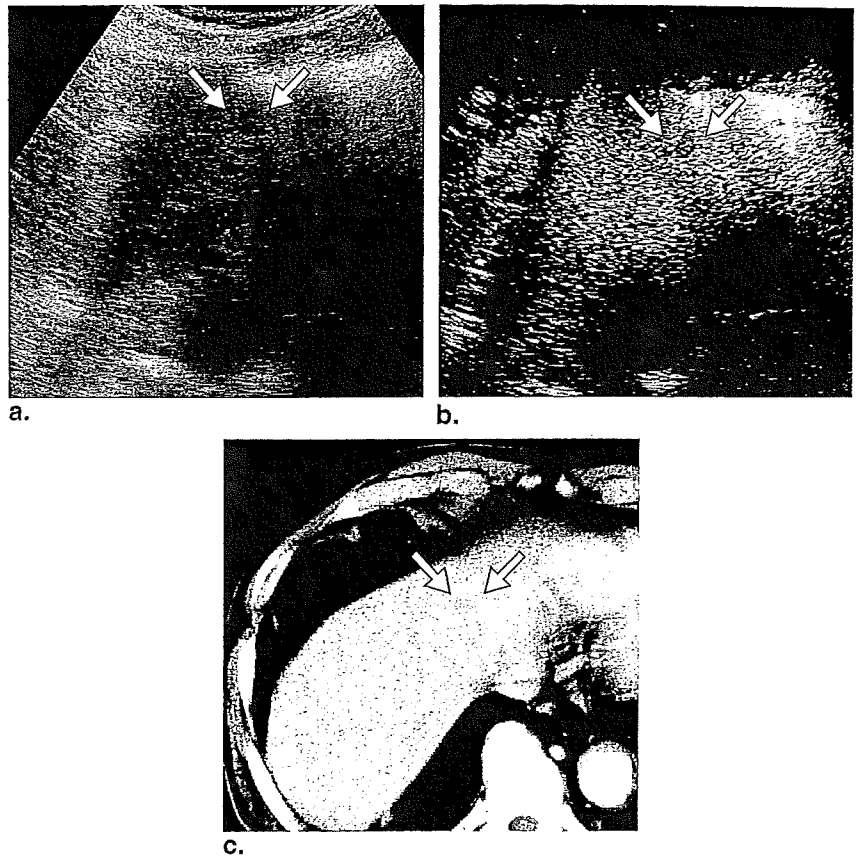

Figure 6. Liver metastasis from stomach cancer in a 78-year-old man. At follow-up computed tomography 2 months later, the lesion showed growth. Hence, the lesion was considered to be a true metastatic tumor. **(a)** B-mode ultrasonographic image obtained in the left lobe of the liver shows a small hypoechoic lesion in segment 4. **(b)** Contrast-enhanced ultrasonographic image in the same region shows a small and subtle signal void without enhancement in segment 4. **(c)** Transverse contrast-enhanced computed tomographic scan shows a small hypoattenuating lesion. All readers overlooked this nodule on both B-mode ultrasonography alone and the combination of B-mode ultrasonography and contrast-enhanced ultrasonography.

Figure 3. By use of contrast-enhanced ultrasonographic images, the average sensitivity for detecting hepatic metastases was improved from 42.1% to 76.4%, and the average number of false positives was reduced from 1.1 to 0.5 per case. For these FROC data, the average FOM values for all physicians increased to a statistically significant degree, from 0.44 without the contrast-enhanced ultrasonographic images to 0.79 with the images ($P < .00001$) (Table 2). It is important that the performances of all physicians were improved when the contrast-enhanced ultrasonographic image was used.

False-positive Findings

False-positive lesions detected in this study corresponded to fibrosis or sequelae, focal fatty sparing or focal fatty change, cyst, or hemangioma (Table 3). The average numbers of false-positive lesions for the 33 cases and seven readers were 35.0 by use of B-mode US alone and 15.1 with combined ultrasonographic imaging. Figure 4 shows an example of a lesion that was correctly diagnosed as benign lesion with the additional use of contrast-enhanced US. Although the average number of false-positive lesions for the 33 cases was clearly reduced, false-positive findings due to cysts were increased by use of contrast-enhanced US from 5.9 to 9.9. Figure 5 shows an example of a cyst that was misdiagnosed as a liver metastasis by five readers on contrast-enhanced US with a high confidence level.

False-negative Findings

One lesion was not detected by any of the readers with B-mode US alone, and also with contrast-enhanced US (Fig 6). With B-mode US alone, 19 lesions in 10 patients were not detected by any of the readers; however, 18 of these lesions were detected by use of contrast-enhanced US with a high confidence level (Figs 7 and 8). Figure 9 shows the

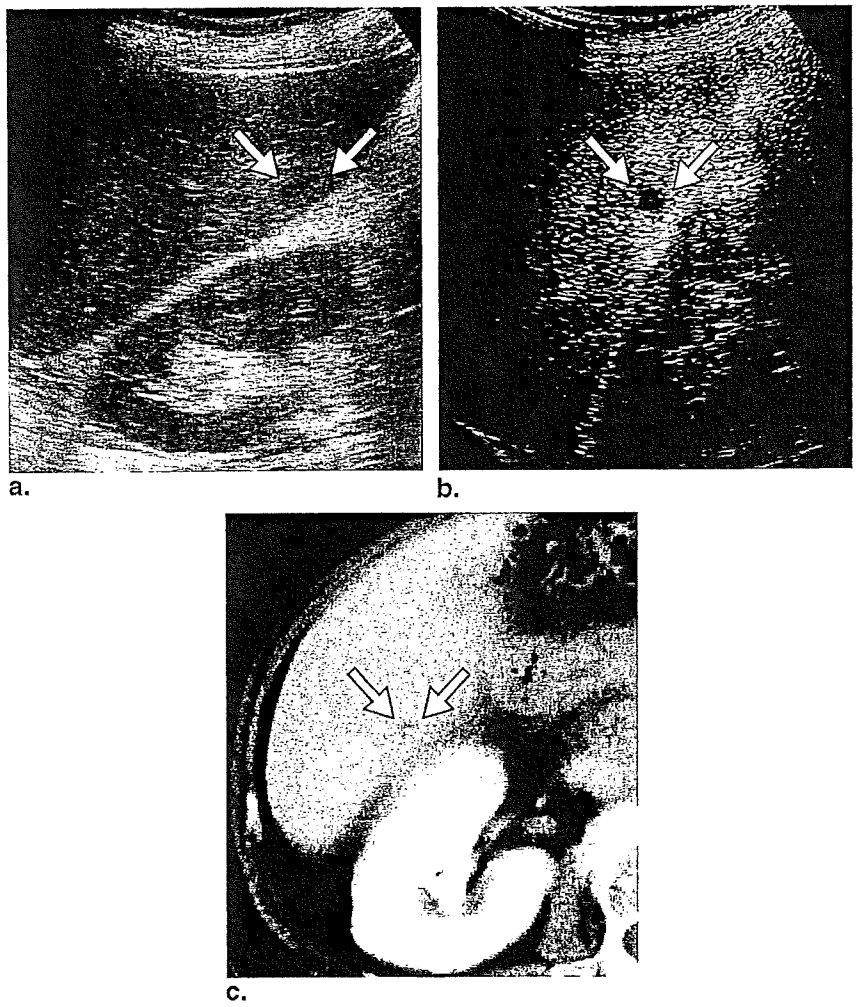

Figure 7. Histologically proved liver metastasis from ovarian cancer in a 73-year-old woman. **(a)** B-mode ultrasonographic image obtained in the right lobe of the liver shows a small and slightly hypoechoic lesion in segment 6. **(b)** Contrast-enhanced ultrasonographic image in the same region shows a small and clear signal void without enhancement in segment 6. **(c)** Transverse contrast-enhanced computed tomographic scan shows a small hypoattenuating lesion. All readers overlooked this nodule at B-mode ultrasonography alone. Conversely, six readers detected the lesion as liver metastasis with high confidence level.

number of false-negative lesions identified by the seven readers. It is important to note that the number of false-negative lesions for all physicians was reduced when the contrast-enhanced ultrasonographic image was used (P = .002, Wilcoxon signed-rank test).

DISCUSSION

We performed an observer study with a free-response ROC procedure by use of ultrasonographic cine clips. To the best of our knowledge, no observer performance study for the detection of liver metastases with ultrasonographic cine clips has been published in the past, although this procedure would be considered very common in the clinical situation. The primary objective of this study was to compare the detection rates of liver metastases without and with use of contrast-enhanced US. As a result, phase-inversion sonography during the liver-specific late phase of contrast enhancement with NC100100 significantly improved the sensitivity, the number of false positives per case, and the FOM value for all readers compared to those with B-mode US alone.

The ability of B-mode US to detect a liver metastasis is limited by the relatively small difference in backscatter between the lesion and the liver parenchyma, which results in poor contrast differentiation between the two tissues. Some metastases show only minimal contrast and are subsequently often not visualized. CT and, to a lesser extent, MR imaging have similar limitations in lesion-to-liver contrast on

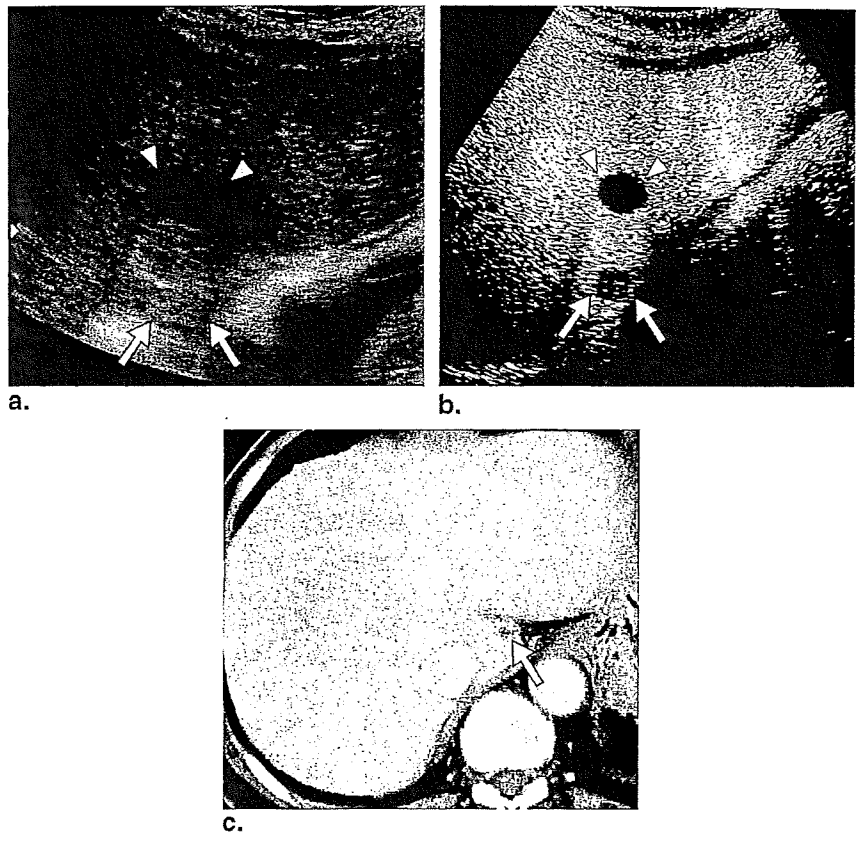

Figure 8. Histologically proved liver metastasis from ovarian cancer in a 74-year-old woman. **(a)** B-mode ultrasonographic image obtained in the right lobe of the liver shows a slightly hyperechoic lesion in segment 1 (*arrows*) and a typical hepatic cyst with sharp margins and increased transmission through the lesion (*arrowheads*). **(b)** Contrast-enhanced ultrasonographic image in the same region shows a clear signal void without enhancement in segment 1 (*arrows*) and a typical hepatic cyst with sharp margins and increased transmission through the lesion (*arrowheads*). **(c)** Transverse contrast-enhanced computed tomographic scan shows a small hypoattenuating lesion (*arrow*). All readers overlooked this nodule at B-mode ultrasonography alone. Conversely, five readers detected the lesion as liver metastasis with high confidence level.

unenhanced images. These techniques, therefore, are routinely performed with the use of contrast agents, and liver-specific MR imaging agents have proven to be particularly useful in this respect (29). Such agents are now also available in the United States. The use of NC100100 in its liver-specific late phase can substantially increase the echogenicity of the liver at pulse-inversion US as the microbubbles accumulate within the normal parenchyma. The echogenicity of metastases, on the other hand, remains unaffected because they do not accumulate the contrast agent in the late phase. Thus, the sensitivity and FOM value for the detection of malignant lesions in this study was improved for all readers with combined use of contrast-enhanced US compared to B-mode US alone.

The average numbers of false positive lesions were also reduced remarkably by contrast-enhanced US compared to B-mode US alone, expect for some cysts. The reason for the relatively low false-positive rate of phase-inversion US is that metastases and benign lesions showed different responses after the administration of the contrast agent. Although all metastases showed no or little late-phase uptake of contrast agent, almost all solid benign lesions showed late-phase enhancement that was similar to that of normal liver parenchyma. Focal fatty changes or sparings generally consist of essentially normal parenchyma and are, therefore, expected to behave like it. Hemangiomas are usually characterized by a gradual filling-in with contrast material over a few minutes on dynamic CT or MR imaging, which may explain why six of seven hemangiomas showed late-phase enhancement on phase-inversion US in this study. Chami et al (13) reported that hypoechoic benign lesions, such as fibrosis or sequelae resulting from metastases that were sterilized by chemotherapy may appear as hypoechoic areas during the portal-to-late phase, which were misdiagnosed as metastases. In this

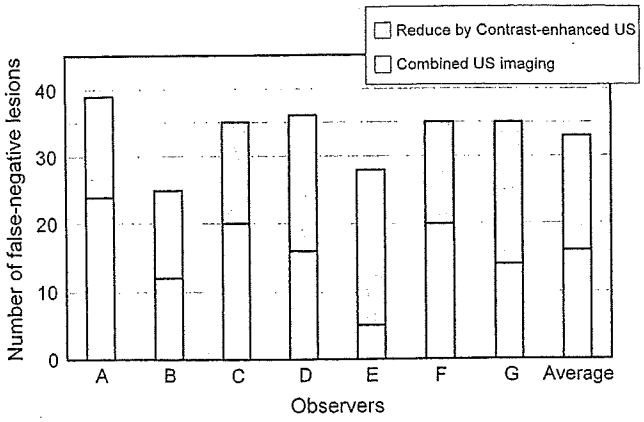

Figure 9. The number of false-negative lesions with and without contrast-enhanced ultrasonography (US) for the seven physicians.

study, however, such lesions did not show clear signal voids without enhancement on late phase images, and that is probably the reason why the average number of false-positive lesions was improved from 23.9 to 5.0 with the additional use of contrast-enhanced US. As for the cysts, one reason for the increase in false-positive results may be related to that seven out of 64 cysts that appeared on B-mode US were considered by many readers as liver metastasis by phase-inversion US as shown in Figure 5, and observers seemed to find it difficult to diagnose these cysts. These could be complicated cysts that may have been accompanied by endocystic septa or hemorrhage.

The underlying mechanism of the selective late uptake of NC100100 by hepatic and splenic parenchyma is not fully understood. One possible explanation is that the microbubbles may be accumulated by Kupffer cells (reticuloendothelial system components of the liver) in healthy parenchyma (30). Alternatively, microbubbles may be entrapped in the liver sinusoids, although it would be difficult to explain why this should also happen in the spleen, which also can display late-phase enhancement but has a different microvasculature.

As shown in Figure 9, the number of false-negative cases was obviously reduced by the additional use of contrast-enhanced US for all observers. However, three nodules were detected in three cases by B-mode US alone, and not by contrast-enhanced US for all observers. These three nodules were located at liver segment 8 inches depth ($\geq$12 cm below the skin). The results may be attributable to the fact that ultrasonographic beam attenuation is far greater in contrast-enhanced US than in B-mode US due to low MR imaging.

Our results would not be compared with the previous ultrasonographic examination results because our results were based on off-site observer study, whereas all previous ultrasonographic results were based on on-site study. However, we may compare our results to previous studies by means of a FROC procedure. Ward et al (31) conducted an observer study to compare the detection of liver metastases by SPIO-enhanced MR imaging and dual-phase CT. The average A_z values by four observers were 0.78 and 0.83 by dual-phase CT and SPIO-enhanced MR imaging, respectively, and the average sensitivities were 75% and 80%, respectively. On the other hand, Onishi et al (32) carried out an observer study to compare the detection of liver metastases by multidetector row CT, SPIO-enhanced MR imaging, and both techniques combined, and the average A_z values by three observers were 0.66, 0.58, and 0.70, respectively, and the average sensitivities were 48%, 43%, and 59%, respectively. By comparison, the average FOM values for the seven observers in the present study were 0.44 and 0.76 by B-mode US alone and combined ultrasonographic imaging, respectively, and the average sensitivities were 41.6% and 72.2%, respectively, which seems to suggest that the results of off-site reading with combined ultrasonographic imaging would be comparable to those by the two studies described above, although the clinical cases used in these studies were different. These findings implicate the possibility that the off-site reading of ultrasonographic images for diagnosis could be practicable in clinical practice.

The present study has some limitations. First, as mentioned in previous studies (31, 32), a potential limitation is the lack of histologic proof for all nodules assumed to be hepatic metastases. However, several clinical findings, including those on contrast-enhanced CT, SPIO-MR imaging, follow-up CT, follow-up MR imaging, and follow-up US, were available for all metastases. The presence of other proved metastases, the small size of many nodules, and/or the patient's clinical history frequently made biopsy of individual lesions unnecessary or impractical. Consequently, the exact number of metastases in each liver could not be determined and, therefore, the specificity and accuracy could not be determined accurately. In theory, it is possible that some false-positive or false-negative lesions may have been included inadvertently.

Second, the number of cases used was small (n = 33) in our study. However, all of the seven observers showed a significantly higher detection rate with contrast-enhanced US than with B-mode US alone.

Third, in this observer study, 57 nodules detected by both contrast-enhanced CT and contrast-enhanced US were selected as the gold standard. However, as described in the Materials and Methods section, 82 nodules were actually detected in total. Technically, these 82 nodules should be used as the gold standard for the observer study. However, 10 nodules detected only by SPIO-enhanced MR imaging were not confirmed by two radiologists and thus, these nodules may be considered non-actionable in US. In addition, we did not compare detection rates among modalities such as CT, MR imaging, and US because no observer study was done with CT and MR imaging. Therefore, we selected the 57

nodules detected by the contrast-enhanced CT and contrast-enhanced US as the gold standard.

In conclusion, the combination of conventional US and contrast-enhanced US during the late liver-specific phase of the microbubble ultrasonographic contrast agent NC100100 showed a higher accuracy in the detection of hepatic metastases than did conventional US alone.

ACKNOWLEDGMENTS

The authors are grateful to Shigeki Ichimura, MD, Masahiko Yamada, MD, Yasuhari Imai, MD, Ryo Metoki, MD, Liu Guang-Jian, MD, Junich Taira, MD, Kaoru Tsuchiya, MD, and Kazunobu Aso, MD, for participating observers, and to Elizabeth Lanzl for improving the manuscript.

REFERENCES

1. Wernecke K, Rummeny E, Bongartz G, et al. Detection of hepatic masses in patients with carcinoma: comparative sensitivities of sonography, CT, and MR imaging. AJR Am J Rentogenol 1991; 157:731–739.
2. Clarke MP, Kane RA, Steele G Jr, et al. Prospective comparison of prospective imaging and intraoperative ultrasonography in the detection of liver tumors. Surgery 1989; 106:849–855.
3. Ohlsson B, Tranberg KG, Lundstedt C, et al. Detection of hepatic metastases in colorectal cancer: a prospective study of laboratory and imaging methods. Eur J Surg 1993; 159:275–281.
4. Frate DC, Zuiani C, Viviana Londero V, et al. Comparing Levovist-Enhanced Pulse Inversion Harmonic Imaging and Ferumoxides-Enhanced MR Imaging of Hepatic Metastases. Am J Roentgenol 2003; 180: 1339–1346.
5. Harvey CJ, Blomley MJK, Eckersley RJ, et al. Hepatic malignancies: improved detection with pulse-inversion US in late phase of enhancement with SH U 508A-early experience. Radiology 2000; 216:903–908.
6. Albrecht T, Hoffmann CW, Schmitz SA, et al. Phase-inversion sonography during the liver-specific late phase of contrast enhancement: improved detection of liver metastases. AJR 2001; 176:1191–1198.
7. Albrecht T, Blomley MJK, Burns PN, et al. Improved detection of hepatic metastases with pulse-inversion US during the liver-specific phase of SH U 508A: multicenter study. Radiology 2003; 227:361–370.
8. Quaia E, Calliada F, Bertolotto M, et al. Characterization of focal liver lesions with contrast-specific US modes and a sulfur hexafluoride-filled microbubble contrast agents: diagnostic performance and confidence. Radiology 2004; 232:420–430.
9. Watanabe R, Matsumura M, Chen CJ, et al. Characterization of tumor imaging with microbubble-based ultrasound contrast agent, Sonazoid, in rabit liver. Biol Pharm Bull 2005; 28:972–977.
10. Watanabe R, Matsumura M, Chen CJ, et al. Gray-scale liver enhancement with Sonazoid (NC100100), a novel ultrasound contrast agent; detection of hepatic tumors in a rabbit model. Biol Pharm Bull 2003; 26: 1272–1277.
11. Forsberg F, Piccoli CW, Liu JB, et al. Hepatic tumor detection: MR imaging and conventional US versus pulse-inversion harmonic US of NC100100 during its reticuloendothelial system–specific phase. Radiology 2002; 222:824–829.
12. Long JA, Daanen V, Moreau-Gaudry A, Troccaz J, Rambeaud LL, et al. Real-time four-dimensional (4D) ultrasound-guided prostatic biopsies a phantom. Comparative study versus 2D guidance. Prog Urol 2007; 17: 1337–1342.
13. Chami L, Lassau N, Malka D, et al. Benefit of contrast-enhanced sonography for the detection of liver lesions: comparison with histologic findings. AJR 2008; 190:683–690.
14. Couinaud C. Le foie: etsudes anatomiques et chirurgicales. Paris, France: Masson, 1957; 9–12.
15. Bismuth H. Surgical anatomy and anatomical surgery of the liver. World J Surg 1982; 6:3–8.
16. Mathieu D, Vilgrain V, Mahfouz A, et al. Benign liver tumors. Magn Reson Imaging Clin N Am 1997; 5:255–288.
17. Mortele KJ, Ros PR. Cystic focal liver lesions in the adult: differential CT and MR imaging features. RadioGraphics 2001; 21:895–910.
18. Horton KM, Bluemke DA, Hruban RH, et al. CT and MR imaging of benign hepatic and biliary tumors. RadioGraphics 1999; 19:431–451.
19. Kim T, Federle MP, Baron RL, et al. Discrimination of small hepatic hemangiomas from hypervascular malignant tumors smaller than 3 cm with three-phase helical CT. Radiology 2001; 219:699–706.
20. Quaia E, Calliada F, Bertolotto M, et al. Characterization of focal liver lesions with contrast-specific US modes and a sulfur hexafluoride-filled microbubble contrast agent: diagnostic performance and confidence. Radiology 2004; 232:420–430.
21. Hirohashi S, Ueda K, Uchida H, et al. Nondiffuse fatty change of the liver: discerning pseudotumor on MR images enhanced with ferumoxides—initial observations. Radiology 2000; 217:415.
22. Kobayashi T, Xu XW, MacMahon H, et al. Effect of a computer-sided diagnosis scheme on radiologists' performance in detection of lung nodules on radiographs. Radiology 1996; 199:843–848.
23. MacMahon H, Engelman R, Behlen FM, et al. Computer-aided diagnosis of pulmonary nodules: results of a large-scale observer test. Radiology 1999; 213:723.
24. Chakraborty DP, Berbaum KS. Observer studies involving detection and localization: modeling, analysis, and validation. Med Phys 2004; 31: 2313–2330.
25. Chakraborty DP, Winter LH. Free-response methodology: alternate analysis and a new observer-performance experiment. Radiology 1990; 174:873–881.
26. Zheng B, Chakraborty DP, Rockette HE, et al. A comparison of two data analysis from two observer performance studies using jackknife ROC and JAFROC. Med Phys 2005; 32:1031–1034.
27. Chakraborty DP. Analysis of location specific observer performance data: validated extensions of the jackknife free-response (JAFROC) method. Acad Radiol 2006; 13:1187–1193.
28. Dorfman DD, Berbaum KS, Mets CE. Receiver operating characteristic rating analysis: generalization to the population of readers and patients with the Jackknife method. Invest Radiol 1992; 27:723–731.
29. Seneterre E, Taourel P, Bouvier Y, et al. Detection of hepatic metastases: ferumoxides-enhanced MR imaging versus unenhanced MR imaging and CT during arterial portography. Radiology 1996; 200:610–611.
30. Watanabe R, Matsumura M, Munemasa T, et al. Mechanism of hepatic parenchyma-specific contrast of microbubble-based contrast agent for ultrasonography: microscopic studies in rat liver. Invest Radiol 2007; 42: 643–651.
31. Ward J, Naik KS, Guthrie JA, et al. Hepatic lesion detection: comparison of MR imaging after the administration of superparamagnetic iron oxide with dual-phase CT by using alternative-free response receiver operating characteristic analysis. Radiology 1999; 210:459–466.
32. Onishi H, Murakami T, Kim T, et al. Hepatic metastases: detection with multi-detector row CT, SPIO-enhanced MR imaging, and both techniques combined. Radiology 2006; 239:131–138.

ELSEVIER

Clinical Imaging 33 (2009) 447–453

CLINICAL IMAGING

Perfusion study of liver lesions with superparamagnetic iron oxide: distinguishing hepatocellular carcinoma from focal nodular hyperplasia

Kazuhiro Saito*, Katsutoshi Sugimoto, Ryota Nishio, Youichi Araki, Fuminori Moriyasu, Dai Kakizaki, Koichi Tokuuye

Department of Radiology, Tokyo Medical University, Tokyo, Japan
Department of Internal Medicine, Tokyo Medical University, Tokyo, Japan

Received 10 November 2008; accepted 14 January 2009

Abstract

We performed a perfusion study with superparamagnetic iron oxide (SPIO) and evaluated the possibility of acquiring hemodynamic imaging in hypervascular hepatocellular nodules. Single-slice computed tomography during arteriography (SCTA) and an SPIO perfusion study were performed and compared. The findings of the direction of blood flow in the lesion and the findings corresponding to the corona enhancement on the SPIO perfusion study agreed well with the findings of SCTA. In conclusion, SPIO perfusion is useful in evaluating the hemodynamics of hypervascular hepatocellular nodules.

Keywords: Corona enhancement; Dynamic study; MRI; SPIO

1. Introduction

Both hepatocellular carcinoma (HCC) and focal nodular hyperplasia (FNH) show hypervascular characteristics on diagnostic imaging. Typically overt HCC shows tumor enhancement in the arterial phase and washout in the equilibrium phase on dynamic computed tomography (CT) and magnetic resonance imaging (MRI) and has capsule-like structure around the tumor [1,2]. FNH is usually lobulated and well circumscribed and has a central stellate scar with radiating fibrous septa. Dynamic study shows enhancement in the arterial phase and isodensity in the equilibrium phase [3,4]. In cases with completely typical findings, the differential diagnosis of both entities is relative easy, but in cases that do not have completely typical findings, the diagnosis is difficult.

FNH displays a specific centrifugal enhancement on angiography, called a spoke-wheel appearance [5]. While this finding can be detected in 57–90% of patients with large lesions, it can be difficult to detect in small lesions [5,6]. Kudo et al. [7] reported excellent detection of this specific vascular structure with dynamic contrast-enhanced ultrasound under infusion of carbon dioxide microbubbles through an angiographic catheter. Miyayama et al. [8] reported the possibility of the detection of these specific hemodynamic features with continuous acquisition of single-slice CT during arteriography (SCTA). However, these methods have the drawback of acquiring invasive angiography. SCTA also shows the drainage vessel indirectly [8,9]. The drainage vessel of hypervascular HCC is the portal vein, and SCTA shows corona enhancement around a tumor [9]. However, the drainage vessel of FNH is the hepatic vein or sinusoid around the nodule [10], and corona enhancement is not always observed.

Superparamagnetic iron oxide (SPIO)-enhanced MRI is a noninvasive modality. SPIO accumulates in Kupffer cells present in normal liver parenchyma and causes a signal loss

* Corresponding author. Tokyo Medical University, 6-7-1 Nishi-Shinjuku, Shinjuku-ku, Tokyo 160-0023, Japan. Tel.: +3 3342 6111; fax: +3 3348 6314.

0899-7071/09/$ – see front matter © 2009 Elsevier Inc. All rights reserved.
doi:10.1016/j.clinimag.2009.01.008

Table 1
Patient demographic data

	HCC (n=11)	FNH (n=10)
SCTA acquisition	9	4
Age in years (mean)	63.8	36.2
Sex (male:female)	6:5	6:4
Underlying liver disease		
None	2	10
HBV	3	0
HCV	5	0
Alcoholic cirrhosis	1	0
Size in millimeters (mean)	45.3	27.3
Confirmation of diagnosis		
Operation	3	1
Biopsy	3	3
Clinical	5	6
Pathological diagnosis		
Well differentiated	2	
Moderately differentiated	3	
Poorly differentiated	0	
Combined	1	
FNH		4

in the liver parenchyma because of T_2 shortening [11]. In HCC, the number of Kupffer cells decrease; thus, SPIO does not accumulate in HCC, and hence, HCC shows hyperintense lesion [12]. On the other hand, the number of Kupffer cells increases in FNH [13], and as a result, SPIO accumulates in the lesion, and thus, the signal of the lesion decreases. While this is useful to distinguish FNH from other lesions [14], sometimes we encounter difficult cases because of only a slight signal decrease.

Thus, we thought that it would be useful to acquire liver lesion images reflecting the hemodynamic status in addition to SPIO-enhanced MRI. The strong susceptibility effect of SPIO enables evaluation of liver lesion vascularity using rapid injection and acquisition echo-planar sequence [15,16]. This method allows acquisition of several slices quickly and repeatedly and makes it possible to grasp the hemodynamics of liver lesions. We performed perfusion studies with SPIO and compared it to SCTA with regard to the possibility of acquiring images reflecting the hemodynamics in HCC and FNH.

2. Materials and methods

This study was performed in accordance with the Helsinki Declaration, and written informed consent was obtained from all patients.

The SPIO perfusion results in 21 patients were evaluated retrospectively. The subjects included 11 HCC (6 men and 5 women, mean age=63.8 years) cases and 10 FNH (6 men and 4 women, mean age=36.2 years) cases. SCTA was also performed in nine HCC cases and four FNH cases. Demographic data are shown in Table 1. Among the 11 HCC cases, 2 had no underlying liver disease, while 3 had hepatitis B, 5 had hepatitis C, and 1 had alcoholic cirrhosis. None of the FNH cases had an underlying liver disease. The confirmation of HCC was by operation in three cases, by percutaneous biopsy in five cases, and clinically in three cases, based on elevation of tumor marker and typical radiologic findings [1]. Pathological diagnoses were well differentiated in two cases, moderately differentiated in five cases, and combined in one case. The confirmation of FNH was by operation in one case, by percutaneous biopsy in three cases, and clinically in six cases by observation of lesion stability for a minimum of 1 year and typical radiologic findings [3–5]. A central scar was observed in three lesions. The dimension of the lesion was measured using the resected specimen or plain T_1-weighted or T_2-weighted images. The dimension of HCC was 45.3±30.3 mm and that of FNH was 27.3±3.8 mm.

2.1. Single-slice CT during arteriography

Angiography-assisted CT was performed with a 16-detector multidetector-row CT (Light Speed 16, General Electric, Milwaukee, MN). After CT during arterial portography and CT hepatic arteriography were performed, celiac arteriography, superior mesenteric arteriography, and common hepatic arteriography were performed, and then the catheter was advanced into the proper, right, or left hepatic artery. SCTA was performed with the infusion of 3 ml of contrast media (Iomeprol, Eizai, Tokyo, Japan, 350 mgI/ml) at a rate of 1 ml/s in the proper, right, or left hepatic artery using a power injector. Two slices at the center of the target lesion were chosen. Scanning began immediately before initiation of the injection of contrast media with 0.8 s per rotation. A 40-s continuous scanning technique [auto mA (max, 440 mA), 120 kVp] without table feed was used to obtain two sections with a thickness of 10 mm, a beam collimation of 20 mm, and a field of view (FOV) of 22–25 cm. The patients were instructed to hold their breath as long as possible during scanning. The images were sorted at each section and observed by both cine mode and manual mode.

2.2. SPIO perfusion study

The interval between angiography-assisted CT and MRI was less than 1 month. The MR examinations were performed with 1.5-T superconducting MR units (Avanto, Siemens, Erlangen, Germany). After T_1-weighted and T_2-weighted images were obtained, the SPIO perfusion study was performed. Bolus injectable ferucarbotran (Resovist, Bayer Schering Pharma, Osaka, Japan) was used. A total dose of 1.4 ml of ferucarbotran was used per patient. Ferucarbotran was rapidly administered at a rate of 2 ml/s by pushing with 40 ml of physiological saline using a power injector. Because the dose of ferucarbotran was very low, it could not be placed in the power injector; therefore, it was pooled in the elongation tube and pushed with physiological saline. For the perfusion study, the echo-planar method (EPI)

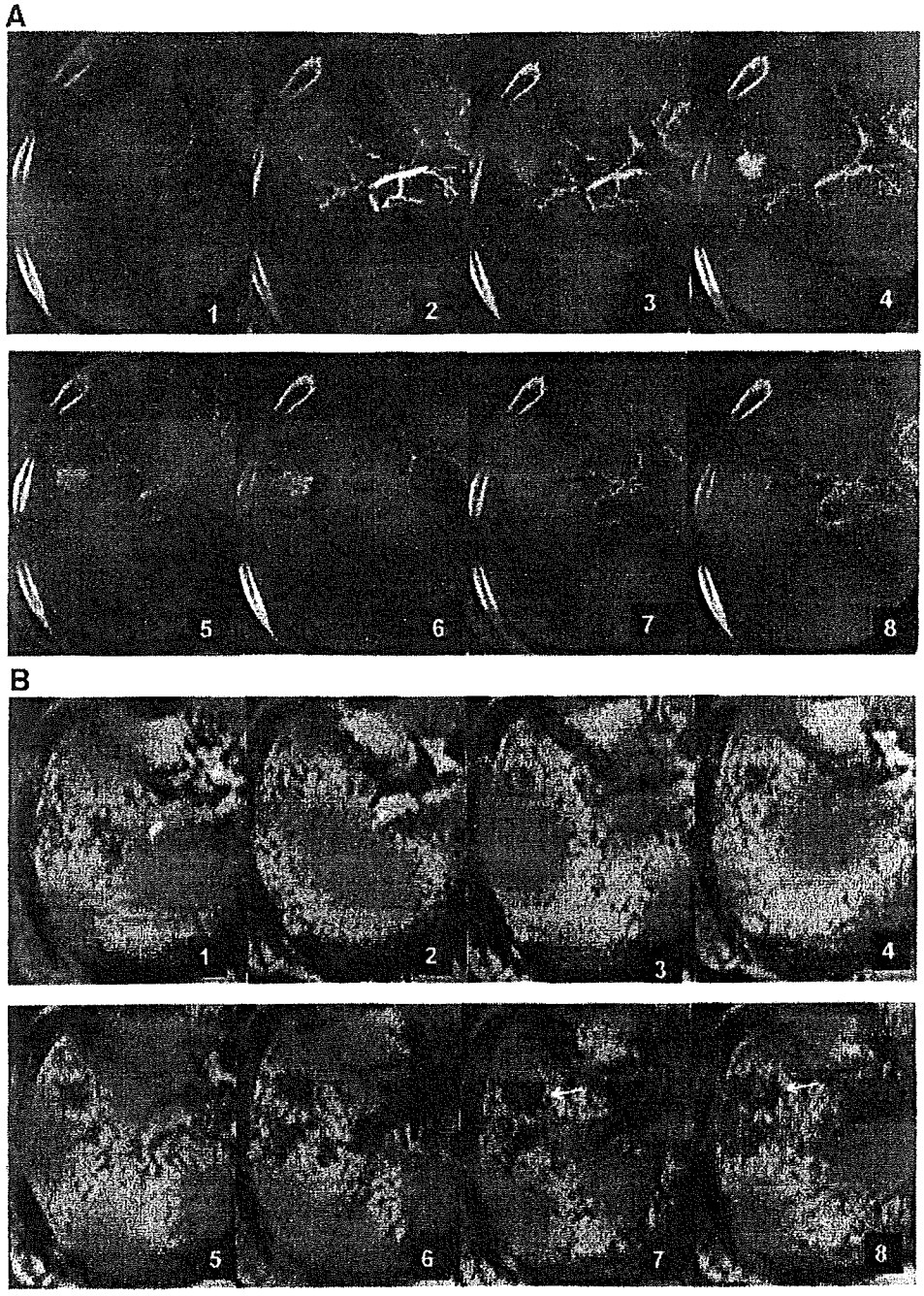

Fig. 1. A 52-year-old man with HCC. (A) SCTA. (B) SPIO perfusion study. SCTA shows centripetal enhancement in the tumor and corona enhancement (arrow). The SPIO perfusion also shows the same enhancement pattern direction and signal reduction in the area surrounding the tumor after transient signal reduction in the tumor (arrowhead). The signal reduction surrounding the tumor corresponds to corona enhancement in SCTA.

was employed. In the 12 initial patients, the scan parameters were as follows: TR, 1150 ms; TE, 20 ms; FA, 70°; EPI factor, 154; matrix, 192×154; bandwidth, 1628 Hz per pixel; FOV, 280–350 mm. Slice thickness was 7 mm. In the sequence using fat saturation and parallel imaging, the generalized autocalibrating partially parallel acquisition algorithm was utilized with an acceleration factor (iPAT factor) of 2. Imaging was obtained before administration of contrast media and 2 s after the start of administration; images were taken during a breath-hold of more than 20 s. Fifteen slice images were obtained per 1.2 s. In the latter nine patients, the scan parameters were changed to improve the time resolution; acquisition slices decreased by six slices and six slice images were obtained per 0.46 s. The scan

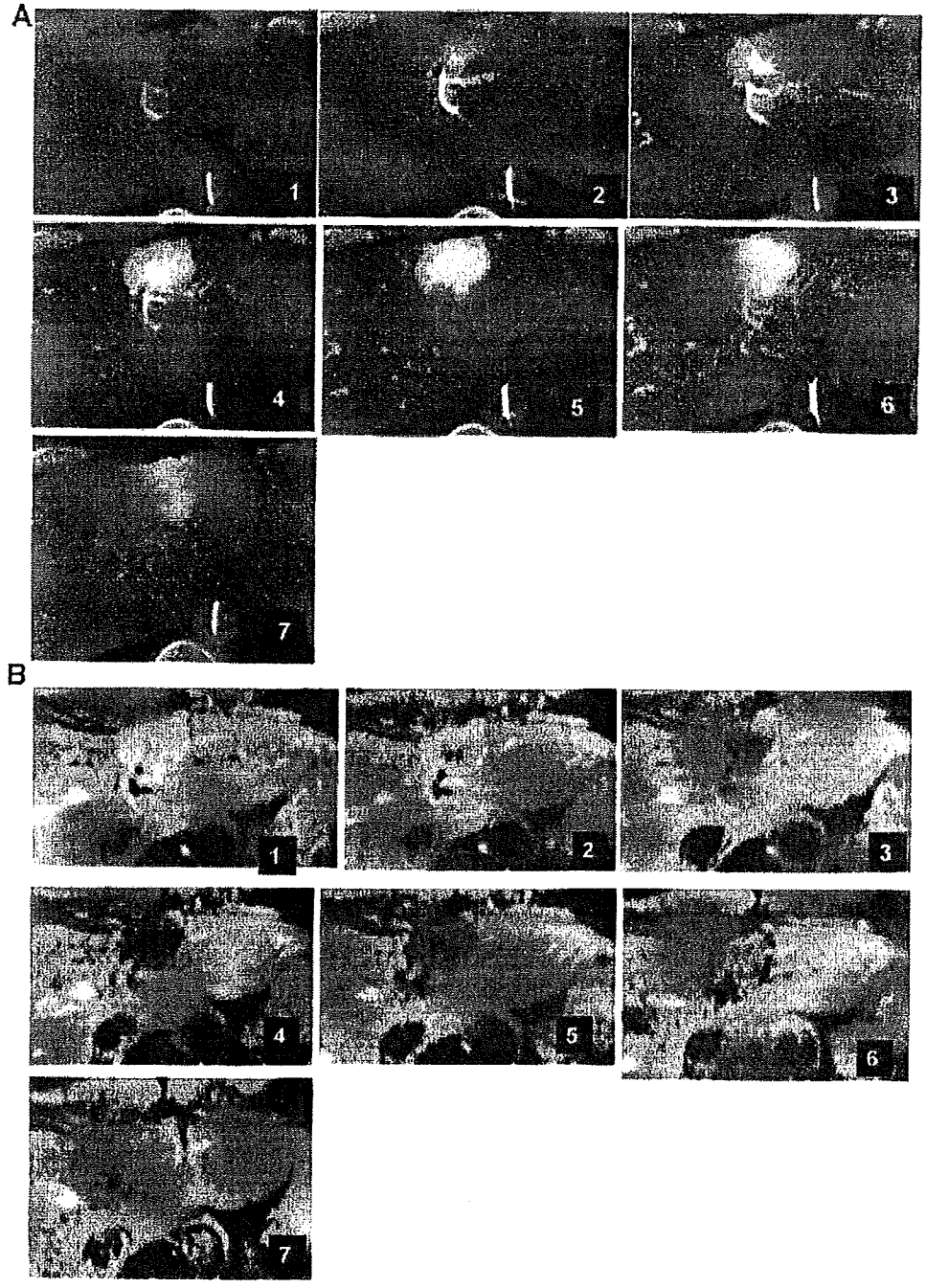

Fig. 2. A 34-year-old man with FNH. (A) SCTA. (B) SPIO perfusion study. SCTA shows centrifugal enhancement in the lesion. Fibrous septa and central scars are observed in the lesion. SPIO perfusion study also shows the same direction of the enhancement pattern. Corona enhancement is not observed by both modalities.

parameters were as follows: TR, 460 ms; TE, 20 ms; FA, 90°; matrix, 192×156. The other parameters remained unchanged. After 3 min of administration, T_1-weighted images were obtained. Ten minutes after administration, T_2-weighted fast spin-echo images and T_2^*-weighted images were taken. The images were sorted at each section and observed by both cine mode and manual mode.

2.3. Image analysis

2.3.1. SCTA versus SPIO perfusion study

SCTA was observed by two doctors whose specialty was liver imaging (16 and 6 years' experience), without patient information. The evaluation item included the vascularity of the lesion, the direction of the enhancement, and the presence

of corona enhancement. The vascularity was classified as hypervascular, isovascular, or hypovascular, in comparison to surrounding liver parenchyma. The direction of the enhancement was classified into centrifugal, centripetal, or all over the lesion simultaneously. Concerning the corona enhancement [8], it was identified as present or absent.

After evaluation of SCTA, we evaluated the SPIO perfusion study without patient information. The evaluation was performed by the same two observers after an interval of more than 2 weeks in order to prevent bias. The rapid decrease in the lesion signal corresponded to the lesion vascularity [15,16]. The evaluation of the enhancement direction in the lesion was the same as that in SCTA, classified into centrifugal, centripetal, or all over the lesion simultaneously. A decrease in the signal of the area surrounding the lesion after the transient signal decrease in the lesion, which corresponded to the corona enhancement, was observed, and any signal changes were recorded.

The two observers evaluated by consensus reading, and in case of disagreement, they had a discussion until a decision was made.

2.3.2. SPIO perfusion study

The vascularity of the lesion, the direction of the enhancement in the lesion, and the presence of the decrease in the signal of the liver parenchyma surrounding the lesion after the transient signal decrease in the lesion were evaluated (n=21 subjects, including those who only underwent SPIO perfusion).

3. Results

3.1. SCTA and SPIO perfusion study

3.1.1. Vascularity of the lesion

All 13 lesions appeared hypervascular on SCTA. All of the lesions showed a rapid decrease in lesion signal on SPIO perfusion (Fig. 1).

3.1.2. Direction of blood flow in the lesion

HCC showed centripetal enhancement in four patients, total enhancement simultaneously in three patients, and centrifugal enhancement in two patients on SCTA. The findings of SPIO perfusion almost completely agreed with the findings of SCTA.

FNH showed centrifugal enhancement in two patients, centripetal enhancement in one patient, and total enhancement simultaneously in one patient (Fig. 2). The findings of SPIO perfusion almost completely agreed with the findings of SCTA.

3.1.3. Corona enhancement

Eight of nine HCC patients showed corona enhancement in SCTA. One patient, whose exophytic lesion was confirmed to be well-differentiated HCC by resection, showed no corona enhancement. The findings of SPIO perfusion substantially agreed with the findings of SCTA (Fig. 1) except for this exophytic lesion.

FNH showed no corona enhancement on SCTA in all four patients. No decrease in the signal of the area surrounding the lesion after rapid decrease in the signal of the lesion was observed on SPIO perfusion (Fig. 2).

3.2. SPIO perfusion study

3.2.1. Vascularity of the lesion

All 21 patients showed a rapid decrease in the lesion signal.

3.2.2. Direction of blood flow in the lesion

Among 11 HCC patients, the enhancement pattern in the lesion was centripetal in 6, total enhancement simultaneously in 3, and centrifugal in 2 patients.

In the 10 FNH patients, the enhancement pattern in the lesion was centripetal in 1, total enhancement simultaneously in 1, and centrifugal in 8 patients.

3.2.3. Corona enhancement

A decrease in the signal of the liver parenchyma surrounding the lesion after the rapid decrease in the signal of the lesion was observed in 10 of 11 HCC. The only lesion in which it was not observed was the exophytic HCC.

No decrease in the signal of the liver parenchyma surrounding the lesion after the rapid decrease in the signal of the lesion was seen in any FNH case.

4. Discussion

We set out to determine whether SPIO perfusion would be effective not only as a contrast medium for FNH and HCC but also to obtain useful hemodynamics information. We supposed that it would be possible to observe the vascular structure in the lesion and of the drainage vein, as in angiography-assisted CT [9], because SPIO perfusion studies could allow repeated scanning of multislices during very short times [15,16]. The spoke-wheel appearance of centrifugal spreading vessels of the feeding artery is a well-known finding in FNH [5]. We expected to observe this finding with SPIO perfusion as well. On the other hand, it has been reported that corona enhancement indicates drainage vessels from the tumor indirectly [8] based on studies of angiography-assisted CT, and we also expected to obtain this finding by SPIO perfusion. SPIO perfusion has the advantages of being less invasive and not involving radiation exposure, in comparison to angiography-assisted CT. Moreover, we expected that SPIO perfusion could provide new additional information.

We confirmed the possibility of the evaluation of tumor vascularity as in previous studies [15,16] and also the possibility of evaluating the direction of tumor enhancement.

The evaluation of the direction of tumor enhancement with angiography-assisted CT and dynamic US under intra-arterial injection of carbon dioxide microbubbles has been reported [7,9], but these examinations could not describe multisections, which makes the description of centrifugal enhancement not necessarily easy. A spoke-wheel appearance was seen in 57–90% of FNH patients [5,6]; thus, not only was it not always possible to detect, but the possibility of false negative results had to be confirmed by multisection scanning as well. SPIO perfusion has the potential to compensate for these faults and, therefore, appears useful.

SPIO perfusion also showed the signal loss in parenchyma surrounding the tumor after transient signal loss of the tumor, which corresponded to corona enhancement in cases of HCC. On the other hand, a signal change corresponding to corona enhancement could not be seen in cases of FNH, and thus, it was possible to evaluate drainage vessels indirectly by the SPIO perfusion study. Fukukura et al. [10] reported that FNH had two drainage pathways: one pathway was venous drainage connected directly to the central or hepatic veins surrounding the lesions, while the other pathway was through the intranodular sinusoids that are connected to sinusoids in the surrounding liver. Ueda et al. [9] observed the contour of the lesion enhancement changing from an irregular shape to a round shape in the late phase of SCTA, and this finding indicated that the drainage was through the intranodular sinusoids that are connected to sinusoids in the surrounding liver. We did not encounter this type, but if the main drainage vessels are through the intranodular sinusoids to sinusoids in the surrounding liver, this might cause signal loss in the surrounding liver. Biopsy may be necessary to diagnose such cases.

In this study, CT was repeated on the same slices every 0.8 s in SCTA, and MRI was repeated on the same slices every 1.15 s in the initial 12 cases. SPIO perfusion had a disadvantage in time resolution; nevertheless, there was no difference in evaluation of the direction of the lesion enhancement. In the last nine cases, SPIO perfusion repeated scanning on the same slices every 0.46 s, and hence, the time resolution of SPIO perfusion was superior to that of SCTA. On the other hand, the spatial resolution of SPIO perfusion was inferior to that of SCTA, but it was enough to evaluate the direction of the lesion enhancement.

Gd-DTPA or SPIO has previously been used for the evaluation of perfusion in tumor [15–17]. Echo-planar sequences were used in all reports. Gd-DTPA is an extracellular contrast media, and it rapidly distributes in extravascular spaces after administration. However, SPIO presents intravascular space in the early phase and is gradually phagocytosed by reticuloendothelial cells. SPIO passes into the tumor vessels and has a transient signal loss because of its susceptibility effect; thus, the contrast medium distributing in extravascular spaces is not desirable. Therefore, contrast medium that is limited to intravascular space is advantageous to observing hemodynamics in and around the tumor. That is why we used SPIO in this study.

The limitation of this study was that we could not compare the findings of SPIO perfusion with resected specimens in detail, but we made a comparison with SCTA, a standard for diagnosis of hemodynamics in hepatic lesions, and were able to show that the findings of SPIO perfusion were comparable with those of SCTA. In this study, the subjects of HCC were overt HCC, and no hypovascular HCC cases were included. Concerning this point, we believe that it would not be difficult to distinguish hypovascular nodules from FNH.

In conclusion, SPIO perfusion is useful to evaluate the hemodynamics of hypervascular hepatocellular nodules and has the advantages of being noninvasive and not involving radiation exposure. SPIO not only is effective as a liver-specific contrast agent but also provides hemodynamics information concerning liver lesions.

References

[1] Itoh K, Nishimura K, Togashi K, Fujisawa I, Noma S, Minami S, Sagoh T, Nakano Y, Itoh H, Mori K. Hepatocellular carcinoma: MR imaging. Radiology 1987;164:21–5.
[2] Yamashita Y, Mitsuzaki K, Yi T, Ogata I, Nishiharu T, Urata J, Takahashi M. Small hepatocellular carcinoma in patients with chronic liver damage: prospective comparison of detection with dynamic MR imaging and helical CT of the whole liver. Radiology 1996;200:79–84.
[3] Mortele KJ, Praet M, Van Vlierberghe H, Kunnen M, Ros PR. CT and MR imaging finding in focal nodular hyperplasia of the liver: radiologic–pathologic correlation. AJR 2000;175:687–92.
[4] Carlson SK, Johnson CD, Bender CE, Welch TJ. CT of focal nodular hyperplasia of the liver. AJR 2000;174:705–12.
[5] Rogers JV, Mack LA, Freeny PC, Johnson ML, Sones PJ. Hepatic focal nodular hyperplasia: angiography, CT, sonography, and scintigraphy. AJR 1981;137:983–90.
[6] Mathieu D, Bruneton JN, Drouillard J, Pointreau CC, Vasile N. Hepatic adenomas and focal nodular hyperplasia: dynamic CT study. Radiology 1986;160:53–8.
[7] Kudo M, Tomita S, Tochio H, Kashida H, Hirasa M, Todo A. Hepatic focal nodular hyperplasia: specific findings at dynamic contrast-enhanced US with carbon dioxide microbubbles. Radiology 1991;179: 377–82.
[8] Miyayama S, Matsui O, Ueda K, Kifune K, Yamashiro M, Yamamoto T, Komatsu T, Kumano T. Hemodynamics of small hepatic focal nodular hyperplasia: evaluation with single-level dynamic CT during hepatic arteriography. AJR 2000;174:1567–9.
[9] Ueda K, Matsui O, Kawamori Y, Nakanuma Y, Kadoya M, Yoshikawa J, Gabata T, Nonomura A, Takashima T. Hypervascular hepatocellular carcinoma: evaluation of hemodynamic with dynamic CT during hepatic arteriography. Radiology 1998;206:161–6.
[10] Fukukura Y, Nakashima O, Kusaba A, Kage M, Kojiro M. Angioarchitecture and blood circulation in focal nodular hyperplasia of the liver. J Hepatol 1998;29:470–5.
[11] Stark DD, Weissleder R, Elizondo G, Hahn PF, Saini S, Todd LE, Wittenberg J, Ferrucci JT. Superparamagnetic iron oxide: clinical application as a contrast agent for MR imaging of the liver. Radiology 1988;168:297–301.
[12] Yamamoto H, Yamashita Y, Yoshimatsu S, Baba Y, Hatanaka Y, Murakami R, Nishiharu T, Takahashi M, Higashida Y, Moribe N. Hepatocellular carcinoma in cirrhotic livers: detection with unenhanced and iron oxide-enhanced MR imaging. Radiology 1995;195:106–12.
[13] Tanaka M, Nakashima O, Wada Y, Kage M, Kojiro M. Pathomorphological study of Kupffer cells in hepatocellular carcinoma and hyperplastic nodular lesions in the liver. Hepatology 1996;24:807–12.

[14] Precetti-Morel S, Bellin MF, Ghebontni L, Zaim S, Opolon P, Poynard T, Mathurin P, Cluzel P. Focal nodular hyperplasia of the liver on ferumoxides-enhanced MR imaging: features on conventional spin-echo, fast spin-echo and gradient-echo pulse sequences. Eur Radiol 1999;9:1535–42.
[15] Ichikawa T, Arbab AS, Araki T, Touyama K, Haradome H, Hachiya J, Yamaguchi M, Kumagai H, Aoki S. Perfusion MR imaging with a superparamagnetic iron oxide using T2-weighted and susceptibility-sensitive echoplanar sequences: evaluation of tumor vascularity in hepatocellular carcinoma. AJR 1999;173:207–13.
[16] Saito K, Shindo H, Ozuki T, Ishikawa A, Kotake F, Shimazaki Y, Abe K. Perfusion study of hypervascular hepatocellular carcinoma with SPIO. Magn Reson Med Sci 2005;4:151–8.
[17] Ichikawa T, Haradome H, Hachiya J, Nitatori T, Araki T. Characterization of hepatic lesions by perfusion-weighted MR imaging with an echoplanar sequence. AJR 1998;170:1029–34.

ELSEVIER

Ultrasound in Med. & Biol., Vol. 36, No. 1, pp. 78–85, 2010

0301-5629/10/$–see front matter

doi:10.1016/j.ultrasmedbio.2009.08.001

● *Original Contribution*

EXPRESSION OF HEAT SHOCK PROTEIN 70 IN RABBIT LIVER AFTER CONTRAST-ENHANCED ULTRASOUND AND RADIOFREQUENCY ABLATION

GUANG-JIAN LIU,*† FUMINORI MORIYASU,* TOMIHIKO HIROKAWA,* MUNIRE REXIATI,* MASAHIKO YAMADA,* and YASUHARU IMAI*

*Department of Gastroenterology and Hepatology, Tokyo Medical University, Tokyo, Japan; and †Department of Medical Ultrasound, Institute of Diagnostic and Interventional Ultrasound, The First Affiliated Hospital of Sun Yat-Sen University, Guangzhou, China

(*Received* 20 *April* 2009; *revised* 20 *July* 2009; *in final form* 5 *August* 2009)

Abstract—Heat shock proteins (HSPs) induced by thermal ablation therapy may help presenting tumor antigen to the host immune system and be a valuable adjuvant in the ablation therapy of liver cancer. This paper described our preliminary study on the expression of HSP70 in rabbit liver after contrast-enhanced ultrasound (CEUS) and radiofrequency (RF) ablation. Twenty-five male New Zealand white rabbits were divided into five groups as: control group (n=5), ultrasound group (n=5), CEUS group (n=5), RF group (n=5) and CEUS + RF group (n=5). Clinical ultrasound and RF ablation equipment were used in the present experiment. Sonazoid was used as the contrast agent. All the animals were sacrificed 24 h after the procedure, and HSP70 was detected by immunohistochemistry staining and Western blot analysis. In the groups without RF ablation, there was no evidence of HSP70 expression in the liver tissue of the control group and ultrasound group, whereas positive HSP70 expression was detected in the liver tissue of the CEUS group, with a mean optical density of 0.33. In the RF and CEUS + RF groups, there were cells showing HSP70 expression in the normal liver tissue far from the ablation region. The mean densities of HSP70 expression were 0.31 in the RF group and 0.35 in the CEUS + RF group, respectively. With regard to the distribution of HSP70 expression of the RF and CEUS + RF groups, the marginal areas were stronger than liver tissue 1 cm away from the margin, and the ablated tissues showed no evidence of HSP70 expression. The mean density of HSP70 expression in the marginal areas were 0.47 in the RF group and 0.42 in the CEUS + RF group, respectively. CEUS using Sonazoid may produce HSP70 expression in the normal liver parenchyma after CEUS examination and RF ablation. (E-mail: moriyasu@tokyo-med.ac.jp) © 2010 World Federation for Ultrasound in Medicine & Biology.

Key Words: **Contrast agent, Ultrasound, Heat shock protein, Radiofrequency ablation.**

INTRODUCTION

Image-guided percutaneous radiofrequency (RF) ablation is one of the most commonly used ablation therapies for liver cancer. Imaging plays an important role in ablation therapy for different purposes such as evaluating the tumor before ablation, targeting and monitoring the tumor during ablation and assessing treatment response after ablation (Claudon et al. 2008; Goldberg et al. 2005). With the development of ultrasound contrast agents (UCAs) and contrast-specific imaging techniques, contrast-enhanced ultrasound (CEUS) has been comparable to contrast-enhanced computed tomography (CECT) or contrast-enhanced magnetic resonance imaging (CEMRI), not only for pretreatment assessment of the lesion but also for postablation follow-up, and CEUS is especially useful for real-time guidance of needle positioning and immediate evaluation of treatment response. Thus, low mechanical index (MI) real-time CEUS has been widely accepted and used in the ablation procedure of liver cancer (Lu et al. 2007).

Thermal ablation therapy such as RF ablation, microwave ablation and laser ablation not only damage the tumor by direct heat injury caused by the thermal energy applied, they also cause some indirect injury to the tumor tissue after the cessation of the energy delivery, including apoptosis, microvascular damage, ischemia–reperfusion injury, Kupffer cell activation, altered cytokine expression and alterations in the immune response (Nikfarjam et al.

Address correspondence to: Fuminori Moriyasu, M.D., Chairman and Professor, Department of Gastroenterology and Hepatology, Tokyo Medical University, 6-7-1 Nishi-Shinjuku, Shinjuku-ku, Tokyo 160-0023. E-mail: moriyasu@tokyo-med.ac.jp